JCTC Journal of Chemical Theory and Computation

pubs.acs.org/JCTC Article

Excitonic Model for Strongly Coupled Multichromophoric Systems: The Electronic Circular Dichroism Spectra of Guanine Quadruplexes as Test Cases

James A. Green, Haritha Asha, Fabrizio Santoro,* and Roberto Improta*

Cite This: https://dx.doi.org/10.1021/acs.jctc.0c01100 Read Online

ACCESS | Metrics & More | Article Recommendations | Supporting Information

ABSTRACT: We here propose a general and flexible approach, based on fragment diabatization, which incorporates charge transfer states and significantly increases the reliability of excitonic Hamiltonians for systems where the chromophores are very close. This model (FrDEx) is used to compute the electronic circular dichroism and absorption spectra of two prototype guanine-rich DNA sequences folded in quadruple helices (GQs), i.e., a fragment of the human telomeric sequence (Tel21, antiparallel), and $(TGGGGT)_4$ (TG4T, parallel). Calculations on different subsets of Tel21 and TG4T, from dimers to tetramers, show that FrDEx provides spectra close to the reference full quantum mechanical (QM) ones (obtained with time-dependent density functional theory), with significant improvements with respect to "standard" excitonic Hamiltonians. Furthermore, these tests enable the most cost-effective procedure for the whole GQ to be determined. FrDEx spectra of Tel21 and TG4T are also in good agreement with the QM and experimental ones and give access to interesting insights into the chemical−physical effects modulating the spectral signals. FrDEx could be profitably used to investigate many other biological and nanotechnological materials, from DNA to (opto)electronic polymers.

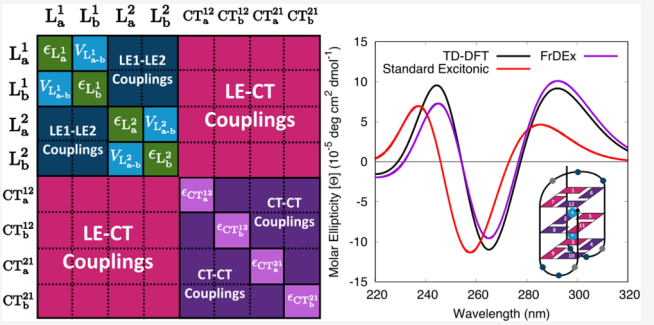

1. INTRODUCTION

Excitonic (Ex) Hamiltonians, such as the Frenkel Hamiltonian, are widely employed cost-effective tools to model photoactivated processes in multichromophoric arrays (MCAs).[1−7] They describe the collective excitations triggered by light in MCAs on the basis of local excitations (LEs) on individual chromophores and the couplings between them. The exciton coupling can be computed as a Coulombic interaction between the transition densities,[8−10] which can be approximated by multipolar expansion, with the interaction between point dipoles[11] being the dominant term at a large distance. This strategy not only avoids resorting to accurate but computationally expensive quantum mechanical (QM) calculations, which cannot be routinely applied to such large systems, but also provides a simple interpretative framework for complex processes. However, Frenkel Hamiltonians should only be applied to weakly coupled bright singlet LEs such that they are "monomer-like", i.e., in MCAs where there is no significant wavefunction (WF) overlap between LEs. Moreover, Frenkel Hamiltonians do not include the coupling with charge transfer (CT) states. Both approximations limit their reliability for many systems/processes, where the chromophores are strongly coupled and/or CT states are key players. In this respect, in the last few years, several procedures have been developed to incorporate CT states into excitonic models of MCAs.[12−22] Extending the range of applicability of excitonic Hamiltonians is a key goal, since in many of the MCAs of biological or technological interest, the chromophores are closely stacked. As a further step forward in this field, we here propose a method that takes into account the perturbation and overlap of LEs due to nearby strongly coupled chromophores, as well as the contributions of CT states. It is based on a fragment diabatization scheme, and hence we name it the Fragment Diabatization-based Excitonic (FrDEx) model. It appears a complete and flexible tool, being able to consider multiple LEs for each site, all possible CT states, as well as interaction terms involving many monomers, herein referred to as "many-monomer effects". In addition to being capable of including all of these effects, it is also possible to switch on and off the different couplings, making it easier to find the most cost-effective approach for the MCA under study and assess the error associated with each choice.

Received: October 19, 2020

As a first, key, application, we compute the electronic circular dichroism (ECD) and the absorption spectra of two representative guanine-rich DNA sequences arranged in quadruple helices (guanine quadruplexes, GQs), each with a different folding topology. The first is a tract of the human telomeric sequence d[$G_3(T_2AG_3)_3$] (hereafter Tel21, antiparallel),[23,24] and the second is the parallel tetramolecular GQ formed by the TGGGGT sequence (hereafter TG4T), both of which are illustrated in Figure 1. DNA is a prototypical

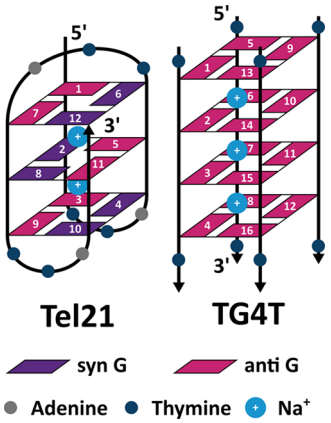

Figure 1. Schematic drawing of the guanine quadruplex structure of Tel21 (antiparallel) and TG4T (parallel).

strongly coupled MCA, and GQ represents an ideal stress test for any excitonic model, since Gs are arranged in closely stacked planar tetrads and two LEs have to be considered for each base. Moreover, GQs are involved in several fundamental biological functions,[25] motivating a strong interest in their intriguing structural properties.[26] Depending on the sequence and several environmental parameters, GQs can adopt many different folding topologies, each with a different ECD signature.[27−30] Any advance in the computation and interpretation of the ECD spectra of GQs is therefore intrinsically relevant. ECD has actually been extensively adopted for the investigation of the supramolecular structure of MCAs since the early stages of the ECD exciton chirality method,[31−38] yet still the simulation of the ECD of strongly coupled MCAs remains a challenge.[37]

Our method provides spectra very close to those obtained at the full QM level used for its parameterization (in this case, time-dependent density functional theory, TD-DFT), and they are in good agreement with the experimental ones, with a meaningful improvement over previous approaches based on Frenkel Hamiltonians with Coulombic couplings (FHC).[39−42] Moreover, we exploit FrDEx to demonstrate how the LEs on each monomer are affected by the large coupling with the surrounding bases, and the influence of the CT states, which determine the peculiar spectral properties of GQs.

2. METHODS

For FrDEx, an excitonic state k for a system of N_{mol} monomers is written as

$$|\Psi^k\rangle = \sum_{m}^{N_{mol}} \sum_{\alpha}^{N_{loc}} C_m^{\alpha,k} |L_\alpha^m\rangle + \sum_{m}^{N_{mol}} \sum_{n\neq m}^{N_{mol}} \sum_{\gamma}^{N_{CT}} C_{mn}^{\gamma,k} |CT_\gamma^{m\to n}\rangle \quad (1)$$

where, for each monomer m, the index α labels the N_{loc} possible LEs (L_α^m) with the corresponding coefficient $C_m^{\alpha,k}$. The index γ identifies the N_{CT} different types of CT states ($CT_\gamma^{m\to n}$) where an electron is transferred from monomer m to monomer n, with the corresponding coefficient $C_{mn}^{\gamma,k}$.

To obtain the energies and couplings of the FrDEx Hamiltonian, we have modified the diabatization procedure introduced by us in ref 43, following a "fragment based" approach, similar to that of Voityuk[44] and Tamura, Burghardt, and Polkehn.[12−16]

In FrDEx, we define diabatic states of some supramolecular complex (SC) consisting of N_{frag} fragments, a subset of the total N_{mol} monomers, using as reference states either the adiabatic states of the fragments (for LEs) or orbital transitions between the fragments (for CT states).

As derived in Section S1 of the Supporting Information (SI), the diabatic states $|\boldsymbol{d}\rangle$ are then obtained by

$$\begin{aligned} |\boldsymbol{d}\rangle &= |\boldsymbol{a}^{SC}\rangle \boldsymbol{D} \\ &= |\boldsymbol{a}^{SC}\rangle \boldsymbol{S}^T (\boldsymbol{S}\boldsymbol{S}^T)^{-1/2} \end{aligned} \quad (2)$$

where $\boldsymbol{S} = \langle \boldsymbol{R}^{frags} | \boldsymbol{a}^{SC} \rangle$ is the overlap of the reference states of the fragments ($|\boldsymbol{R}^{frags}\rangle$) with the adiabatic states of the SC ($|\boldsymbol{a}^{SC}\rangle$). The diabatic energies and couplings can then be calculated from the transformation matrix $\boldsymbol{D}$ applied to the diagonal matrix of adiabatic energies of the SC $H(\boldsymbol{a}^{SC})$

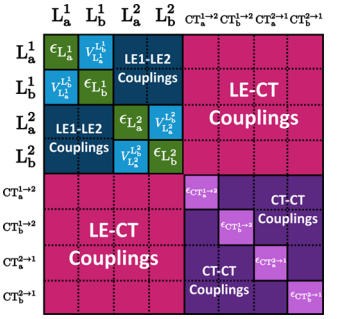

Figure 2. Diagram for the energies and couplings obtained by the FrDEx diabatization performed on two monomers (1 and 2) with two kinds of LE (L_a and L_b) and two kinds of the CT state (CT_a and CT_b).

$$H(\boldsymbol{d}) = \boldsymbol{D}^T H(\boldsymbol{a}^{SC}) \boldsymbol{D} \quad (3)$$

A diagrammatic representation of the energies ϵ and couplings V obtained from a diabatization on a dimer is shown in Figure 2, with just two types of LE and CT states illustrated for simplicity.

More explicitly, the FrDEx Hamiltonian for an entire MCA, including only two-monomer CT−CT couplings (more explanation on this point is found below), may be written as

https://dx.doi.org/10.1021/acs.jctc.0c01100
J. Chem. Theory Comput. XXXX, XXX, XXX−XXX

$$
\begin{aligned}
H_{\mathrm{exc}} &= H_{\mathrm{intra}} + H_{\mathrm{inter}} \\
H_{\mathrm{intra}} &= \sum_{m}^{N_{\mathrm{mol}}} \left\{ \sum_{\alpha}^{N_{\mathrm{loc}}} [\epsilon_{\mathrm{L}_\alpha^m} |\mathrm{L}_\alpha^m\rangle\langle \mathrm{L}_\alpha^m| + \sum_{\beta\neq\alpha}^{N_{\mathrm{loc}}} V_{\mathrm{L}_\alpha^m}^{\mathrm{L}_\beta^m} (|\mathrm{L}_\alpha^m\rangle\langle \mathrm{L}_\beta^m| + \mathrm{hc})] \right\} \\
H_{\mathrm{inter}} &= \sum_{m}^{N_{\mathrm{mol}}} \sum_{n\neq m}^{N_{\mathrm{mol}}} \left\{ \sum_{\alpha,\beta}^{N_{\mathrm{loc}}} V_{\mathrm{L}_\alpha^m}^{\mathrm{L}_\beta^n} (|\mathrm{L}_\alpha^m\rangle\langle \mathrm{L}_\beta^n| + \mathrm{hc}) + \sum_{\gamma}^{N_{\mathrm{CT}}} [\epsilon_{\mathrm{CT}_\gamma^{m\to n}} |\mathrm{CT}_\gamma^{m\to n}\rangle\langle \mathrm{CT}_\gamma^{m\to n}| + \sum_{\delta\neq\gamma}^{N_{\mathrm{CT}}} V_{\mathrm{CT}_\gamma^{m\to n}}^{\mathrm{CT}_\delta^{m\to n}} (|\mathrm{CT}_\gamma^{m\to n}\rangle\langle \mathrm{CT}_\delta^{m\to n}| + \mathrm{hc}) \right. \\
&\quad \left. + \sum_{\delta}^{N_{\mathrm{CT}}} V_{\mathrm{CT}_\gamma^{m\to n}}^{\mathrm{CT}_\delta^{n\to m}} (|\mathrm{CT}_\gamma^{m\to n}\rangle\langle \mathrm{CT}_\delta^{n\to m}| + \mathrm{hc}) + \sum_{\alpha}^{N_{\mathrm{loc}}} (V_{\mathrm{L}_\alpha^m}^{\mathrm{CT}_\gamma^{m\to n}} (|\mathrm{L}_\alpha^m\rangle\langle \mathrm{CT}_\gamma^{m\to n}| + \mathrm{hc}) + V_{\mathrm{L}_\alpha^m}^{\mathrm{CT}_\gamma^{n\to m}} (|\mathrm{L}_\alpha^m\rangle\langle \mathrm{CT}_\gamma^{n\to m}| + \mathrm{hc}))] \right\}
\end{aligned}
\tag{4}
$$

where hc stands for Hermitian conjugate. This Hamiltonian is similar to other ones involving CT states, such as those employed by Tamura, Burghardt, and Polkehn,[12−18] as well as by Cupellini et al.[21,22] and Li et al.[19] in recent studies of the absorption spectra of light harvesting systems. The procedure we use to find the optimal parameters for the Hamiltonian, however, entails some relevant differences.

In our approach, we split the Hamiltonian into an intramolecular part, H_{intra}, and an intermolecular part, H_{inter}. In the intramolecular part, we have the LE energies, $\epsilon_{\mathrm{L}_\alpha^m}$, and the couplings of different LEs on the same monomer, $V_{\mathrm{L}_\alpha^m}^{\mathrm{L}_\beta^m}$. These couplings (highlighted in light blue in Figure 2a for the dimer) are zero in a monomer but become nonzero in an MCA due to the electrostatic influence of the surrounding monomers and/or the overlap with their molecular orbitals, causing LEs defined on an isolated monomer to mix when other monomers are present nearby. This effect has also been discussed in ref 19. Furthermore, the $\epsilon_{\mathrm{L}_\alpha^m}$ values are typically equal to that found in the isolated monomer in "standard" excitonic models, but they can also be influenced by the electrostatic effect of surrounding monomers in an MCA. In the following, we will refer to both these phenomena that affect the LEs as a "perturbation" of H_{intra}.

In the intermolecular part, we have the CT energies $\epsilon_{\mathrm{CT}_\gamma^{m\to n}}$; the couplings between the LE and CT states $V_{\mathrm{L}_\alpha^m}^{\mathrm{CT}_\gamma^{m\to n}}$ (the CT creates a hole in the same monomer involved in the LE) and $V_{\mathrm{L}_\alpha^m}^{\mathrm{CT}_\gamma^{n\to m}}$ (the CT state transfers an electron to the same monomer involved in the LE); and the LE−LE couplings between LEs on different monomers, $V_{\mathrm{L}_\alpha^m}^{\mathrm{L}_\beta^n}$. For simplicity, only two-monomer CT−CT couplings are included in eq 4. In other words, we considered those between CT states in which one is transferring an electron from monomer m to monomer n and the other is transferring an electron from monomer n to monomer m with $V_{\mathrm{CT}_\gamma^{m\to n}}^{\mathrm{CT}_\delta^{n\to m}}$, and those between different types of CT states in which they both transfer an electron from monomer m to n with $V_{\mathrm{CT}_\gamma^{m\to n}}^{\mathrm{CT}_\delta^{m\to n}}$.

The three-monomer ($V_{\mathrm{CT}_\gamma^{m\to n}}^{\mathrm{CT}_\delta^{m\to p}}$ and $V_{\mathrm{CT}_\gamma^{m\to n}}^{\mathrm{CT}_\delta^{p\to n}}$) and four-monomer ($V_{\mathrm{CT}_\gamma^{m\to n}}^{\mathrm{CT}_\delta^{p\to q}}$) CT couplings are thus lacking. However, these latter terms can also be easily computed and considered, by using in the diabatization an SC consisting of three/four or more monomers, as shown in the Results section.

The flexibility of the FrDEx method lies in the ability to choose an SC of any size to compute the couplings and energies, so as to balance computational cost and accuracy, avoiding, at the same time, any double-counting effect. As reported in the Results section, we explore this feature testing different choices of SC to find the optimal parameterization for the H_{intra} and H_{inter} parts of the Hamiltonian.

For the calculation of the spectra, the electric $\boldsymbol{\mu}$ and magnetic $\mathbf{m}$ transition dipole moments of the diabatic states are obtained via the transformation matrix $\mathbf{D}$ applied to the transition dipole moments of the adiabatic states of the SC chosen for the diabatization, in the same manner as eq 3. For the calculation of the rotational strength, we follow the procedure previously put forward by Jurinovich et al.[39−42] and also choose to use the velocity gauge so as to obtain an expression that is origin-independent:

$$
R_{0k}^{\mathrm{v}} = \mathrm{Im}\left[\sum_{\zeta,\eta}^{N_{\mathrm{diab}}} C_\zeta^k C_\eta^k \frac{\nu_{0\zeta}}{\nu_{0k}} [\boldsymbol{\mu}_{0\zeta}^{\mathrm{v}} \cdot \mathbf{m}_{0\eta}] \right] \tag{5}
$$

In the above, the LE and CT states have been grouped together in the double sum over N_{diab} diabatic states, the superscript "v" specifies that $\boldsymbol{\mu}$ (and R) is computed in the velocity gauge, ν_{0k} is the transition frequency of the excitonic state k, and $\nu_{0\zeta}$ is the transition frequency of the diabatic state ζ. For further details, see Section S2 in the SI.

3. COMPUTATIONAL DETAILS

In principle, any QM method can be used to parameterize the FrDEx Hamiltonian, by simply changing the way the matrix $\boldsymbol{S}$ is computed. Due to the size of the GQ, we choose TD-DFT M052X/6-31G(d) calculations to have a full QM reference of the entire GQ, including solvent effect (water) with the polarizable continuum model (PCM).[45] All TD-DFT calculations were performed using the Gaussian 16 package,[46] with the couplings for the FHC model calculated using the "EET" option.[10]

The structure of Tel21 was taken from the first NMR structure of PDB code 143D,[47] while that of TG4T from PDB code 244D.[48] The 143D structure already contained valence hydrogens and had been refined by distance-restrained molecular dynamics, so we did not make any changes to the overall structure. The structure of 244D does not contain valence hydrogens and is from X-ray diffraction data, so valence hydrogens were added, and a partial geometry optimization performed at the PCM (water)/M052X/6-31G(d)/Molecular Mechanics (MM) level.[49] The partial geometry optimization also predicted a "more symmetrical" TG4T structure than that obtained directly from the PDB such that we could test whether a reduction in parameters for FrDEx was possible (see SI Figure S5). Furthermore, geometry optimization leads to a further decrease of the average stacking distance, providing a more stringent test for our procedures. For both structures, before the TD-DFT calculations were performed, all nucleobases except the guanines in the tetrads were removed, along with the sugar

https://dx.doi.org/10.1021/acs.jctc.0c01100
J. Chem. Theory Comput. XXXX, XXX, XXX−XXX

rings and inner Na^+ ions. Their effects could be considered in our model if required, for example, at the QM/MM level. Following this, each of the guanines in the tetrads was replaced by a 9-methyl-guanine (mG), geometry-optimized at the M052X/6-31G(d)/PCM(water) level of theory, by minimizing the RMSD between them.

The diabatizations were performed with an in-house code, available from the authors on request. The spectra for both excitonic methods were calculated using a modified version of the EXAT program,[40,41] with various scripts interfacing the diabatization code for FrDEx to produce the required input for EXAT.

All of the calculated spectra are shifted by −0.85 eV, i.e., the amount necessary to superimpose the PCM/TD-M052X/6-31G(d) spectrum of mG in water onto the experimental one (see Figure S1 in the SI).[50] Applying always the same shift, we can rigorously check the ability of our method to reproduce the effect of the stacking arrangement typical of each GQ fold on the shape and position of its spectrum.

4. RESULTS

4.1. Test Calculations on Smaller Systems. As discussed in Section 2, the flexibility of FrDEx lies in the possibility to choose an SC of any size in the diabatization to parameterize the Hamiltonian. Applying the diabatization to an SC as large as the GQ would provide the full Hamiltonian expressed on the basis of the monomer-like LEs, CT states, and coupling between them. On the other hand, retaining only a subset of LE/CT couplings, thus reducing the dimension of the SC used for the diabatization, could allow significant savings in computational time with a small loss in accuracy. This choice is obviously system-dependent, and FrDEx permits one to easily check for the expected error of any approximation.

4.1.1. Dimers. As a first step, we start analyzing three representative stacked dimers from Tel21 and TG4T with different stacking geometries and interbase stacking distances, as shown in Figure 3. It will be simpler to assess the importance of the different interactions in determining the spectral shape for these dimers than for the full GQ, while, at the same time, these tests will provide important indications on the most suitable methodological approach for the study of the GQ.

Computing the ECD of GQ in the UVC-UVB requires that the two lowest bright $\pi\pi^*$ states of G, commonly referred to as the L_a and L_b states,[51] are explicitly considered.

For what concerns the CT states, FrDEx allows us to consider any possible transition between filled orbitals of a monomer and empty ones in another. We tested different numbers of CT states (see Figure S6 in the SI), and we choose to include the transitions between the frontier orbitals (two filled, three empty) involved in L_a and L_b states, for a total N_{CT} = 6 types of CT states (nb this leads to 12 CT states for every pair, since we have N_{CT} from one monomer to another, and vice versa). This procedure was determined to be the optimal mix of accuracy and efficiency; it indeed provides spectra more accurate than those obtained by considering a smaller number of CT states, and, at the same time, very close to those including additional types of CT states. Concerning this latter point, it is worth remembering that for greater numbers of CT states, a larger number of adiabatic states of the SC would be needed for the transformation in eq 2, increasing the computational cost. From a general point of view, the combination of FrDEx with a suitable analysis tool of the wavefunction, e.g., TheoDORE,[52,53] could also help choose the SC and the number of LE/CT states to include.

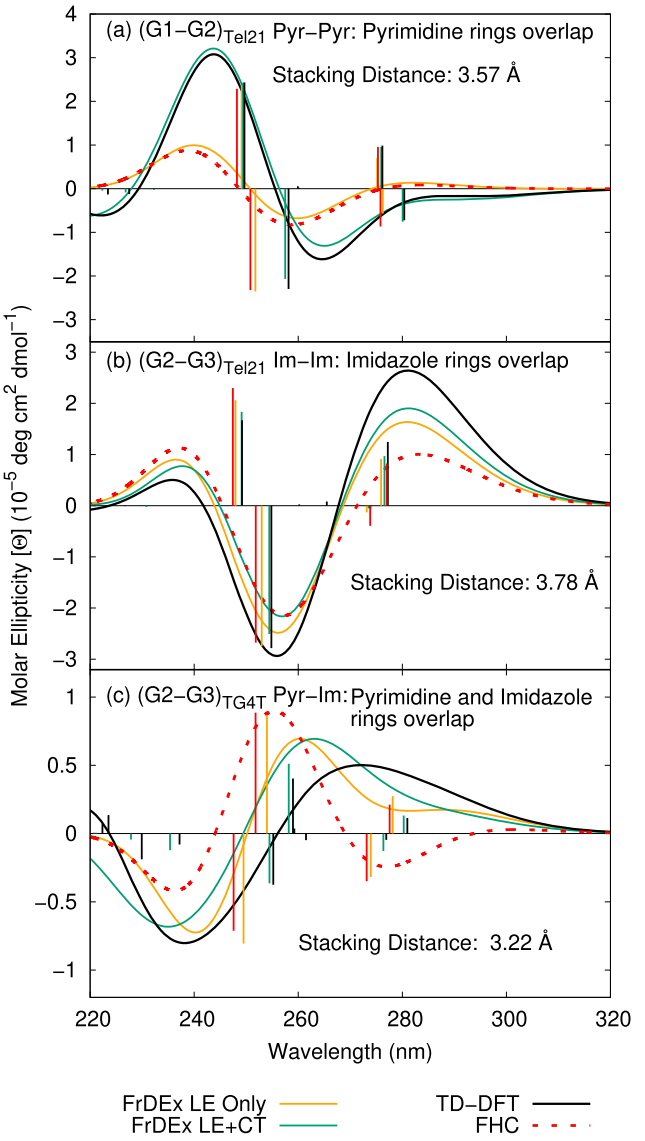

Figure 3. ECD spectra for selected stacked pairs from Tel21 and TG4T. The interbase stacking distance is defined as the component of the absolute distance between the centroids of the bases that is perpendicular to the plane of the bases.

In Figure 3, we compare the spectra provided by FrDEx, FHC, and TD-DFT calculations. We report FrDEx spectra including in the Hamiltonian either only LEs or both LE and CT states, so as to illustrate separately the effect of H_{intra} perturbation on the LEs, and the addition of CT states. Note that any difference between FrDEx "LE only" and FHC spectra is entirely due to the perturbation of H_{intra}. When CT couplings are not considered, for a dimer, the LE−LE coupling terms in H_{inter} are almost equivalent for FHC and FrDEx calculations (see SI Figure S10).

For G1−G2 from Tel21 (panel (a)), inclusion of CT states is necessary for a correct description of the high-energy positive peak at ∼240 nm, whereas the effect of H_{intra} perturbation due to the surroundings is very small. This result can be explained by the larger contribution of CT states in the high-energy region. Interestingly, the FHC method is

https://dx.doi.org/10.1021/acs.jctc.0c01100
J. Chem. Theory Comput. XXXX, XXX, XXX−XXX

able to capture the sign of the rotatory strength of the different transitions but significantly underestimates the splitting between the positive/negative eigenstates, likely due to the neglect of CT states. As a consequence, their positive/negative contributions cancel out, leading to a very shallow ECD spectrum.

For the G2−G3 pair from Tel21 (panel (b)), the opposite is true, i.e., considering the H_{intra} perturbation due to the stacked bases is necessary to improve the agreement with TD-DFT results, whereas inclusion of the CT states has a smaller, though still notable effect. Interestingly, this pair is less closely stacked than G1−G2, indicating that the relative importance of the different effects is governed by the "overall" stacking geometry of the pair and not only by the mere interbase distance. In this case, the severe underestimation of the positive peak at ∼280 nm by FHC is mainly due to the wrong description of the relative intensity of the positive/negative contributions in that energy window. This underestimation is not fully recovered by FrDEx, indicating that inclusion of further LE or CT states may be necessary. As we show in the SI, increasing N_{CT} to 8 produces only a minor improvement, so it is likely that a very large number is needed to perfectly account for the larger orbital overlap/delocalization.

For the G2−G3 dimer extracted from TG4T (panel (c)), the FHC spectrum is very different from the full QM reference, likely due to the strong overestimation of the negative rotatory intensity of the transition at 275 nm. Both the perturbation of H_{intra} and inclusion of the CT states lead the FrDEx calculation to improve the agreement with the TD-DFT spectrum, albeit this agreement is not perfect. This pair has the closest stacking distance of the three examples, and inclusion of additional CT/LE states may be necessary to more accurately consider the larger orbital overlap/delocalization. Similar to the G2−G3 dimer from Tel21, increasing N_{CT} to 8 produces a minor improvement, so once more it is likely that a very large number is needed to perfectly account for the larger orbital overlap/delocalization.

For the distant dimer G1−G3 from Tel21, CT states only have a limited effect (see Figure S6 in the SI), suggesting that it may not be necessary to include those pairs that are well separated in the full GQ.

Hydrogen bonding can also affect H_{intra}. Since ECD spectra of hydrogen-bonded dimers are not intense (see Figure S7 in the SI), this effect can be more easily appreciated by directly comparing the H_{intra} parameters obtained for G2 with different SCs used in the diabatization, as shown in Table 1. Hydrogen bonding (see the G2−G5 dimer) causes a larger redshift of the L_a and L_b energies relative to the monomer than the stacking interactions (G1−G2 and G2−G3), and a much larger value for the intramonomer L_a−L_b coupling (i.e., L_a and L_b of an isolated guanine mix due to the H-bond).

4.1.2. Stacked Trimers and Tetramers. In the next step, we shall analyze in detail the spectra of a representative trimer (G1−G2−G3 from Tel21 as labeled in Figure 1), to get insights into the importance of three-monomer effects, which can also guide us in the choice of the most suitable SC for studying the whole GQ. In principle, considering a trimer would include three-monomer effects in the calculation of couplings between CT states (see also Li et al.[19]), due to the effect of G3 on the CT transitions involving G1 and G2.

Figure 4 reports the ECD spectra of the G1−G2−G3 stacked trimer in Tel21 calculated by TD-DFT, FHC, and FrDEx, but using different levels of approximation. For the purple spectrum, H_{inter} and H_{intra} are obtained by diabatization on the entire trimer, and thus three-monomer terms $V^{CT_\delta^{m\to p}}_{CT_\gamma^{m\to n}}$ and $V^{CT_\delta^{p\to n}}_{CT_\gamma^{m\to n}}$ are also accounted for. This spectrum, as could be expected, is the closest to the TD-DFT reference. However, the contribution of three-monomer terms is small, as shown by its similarity with the brown spectrum, where H_{inter} and H_{intra} are still computed from the entire trimer, but three-monomer couplings are set to zero. Analogously, the error found computing H_{inter} from dimers (light blue curve) appears small, whereas the choice of the SC used for H_{intra} appears more critical. Indeed, the green curve, where both H_{intra} and H_{inter} are computed from dimers, exhibits more significant discrepancies with respect to the TD-DFT spectrum, especially concerning the relative intensity of the two positive lobes. Finally, as shown in the SI (Figure S8), while the inclusion of CT states is a key ingredient to improve the spectra, the coupling between distant G1 and G3 bases does not play a significant role.

To obtain indications on the importance of four-monomer terms, we computed the ECD spectra of two tetramers extracted from TG4T: the stacked tetramer G1−G2−G3−G4,

Table 1. H_{intra} Parameters (LE Energies and Intramonomer L_a−L_b Couplings) for G2 from Tel21, Obtained Using Different SCs

SC	$\epsilon_{L_a^2}$ (eV)	$\epsilon_{L_b^2}$ (eV)	$V^{L_b^2}_{L_a^2}$ (meV)
monomer	5.355	5.814	0
G1−G2	5.346	5.798	3.54
G2−G3	5.365	5.797	−14.61
G2−G5	5.339	5.793	88.07
average	5.356	5.807	12.23
dimers			
G1−G2−G3	5.348	5.771	−10.15
trimer			
G2−G5−G11−G8	5.351	5.768	110.40
tetrad			
G1−G2−G3−G5−G8	5.334	5.681	95.17
HB + stack			

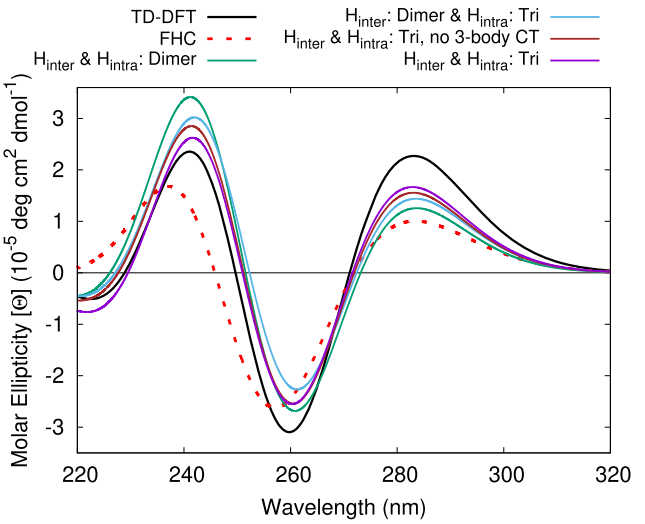

Figure 4. ECD spectra for the G1−G2−G3 stacked trimer of Tel21 computed by TD-DFT, FHC, and FrDEx. For FrDEx, different sizes of SC are used in the calculation of the H_{inter} and H_{intra} portions of the Hamiltonian. See text for further details.

https://dx.doi.org/10.1021/acs.jctc.0c01100
J. Chem. Theory Comput. XXXX, XXX, XXX−XXX

and the hydrogen-bonded and stacked tetramer G2−G3−G6−G7. These are shown in Figure 5. To differentiate the

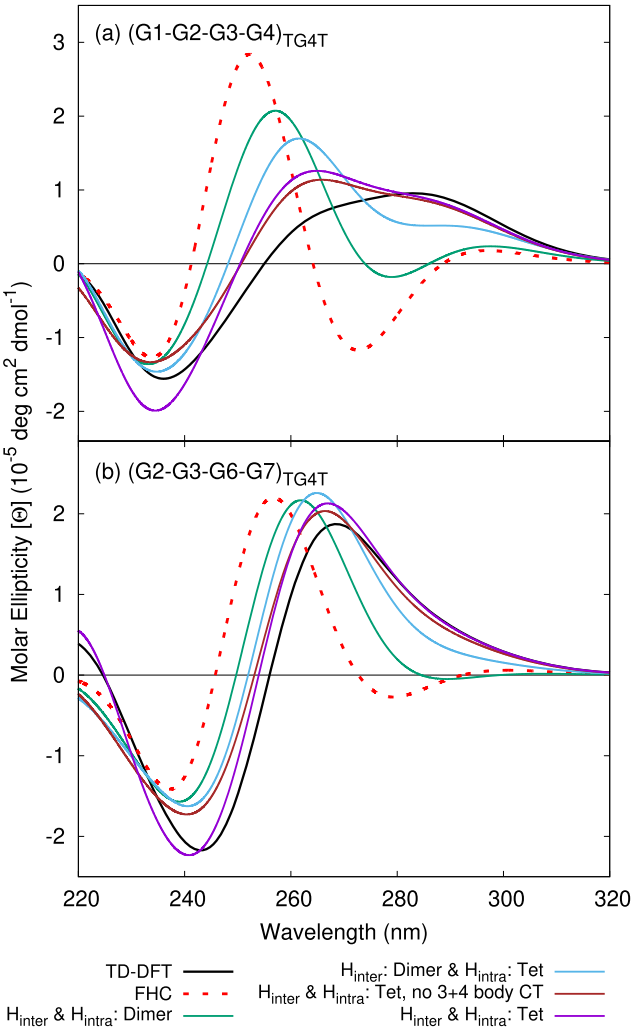

Figure 5. ECD spectra for the (a) G1−G2−G3−G4 stacked tetramer of TG4T and (b) G2−G3−G6−G7 hydrogen-bonded stacked tetramer of TG4T computed by TD-DFT, FHC, and FrDEx. For FrDEx, different sizes of SC are used in the calculation of the H_{inter} and H_{intra} portions of the Hamiltonian. See text for further details.

FrDEx spectra, we use a color code similar to that just adopted for trimers. The purple and brown spectra are obtained using the full tetramer for both H_{inter} and H_{intra}. However, the purple spectrum includes three- and four-monomer CT couplings ($V_{CT_\gamma^{m\to p}}^{CT_\delta^{p\to q}}$, $V_{CT_\gamma^{m\to n}}^{CT_\delta^{p\to n}}$, and $V_{CT_\gamma^{m\to n}}^{CT_\delta^{p\to q}}$), while these couplings are set to zero to obtain the brown spectrum. Dimers were used for H_{inter}, and the tetramer was used for H_{intra} to compute the light blue spectra. Finally, when H_{inter} and H_{intra} are computed on dimers, we obtain the green spectra.

These tetramers provide a rather stringent test due to the close stacking of the bases in TG4T. The agreement between FHC and TD-DFT spectra is indeed rather poor, in particular with regard to the low-energy peak. For both tetramers, FHC incorrectly predicts the appearance of a negative lobe at 270−280 nm. All of the FrDEx calculations improve the agreement with TD-DFT reference. In particular, the notable changes between the green and light blue curves for the low-energy peaks suggest that computing H_{intra} from a tetramer SC allows us to account for important effects. The "more accurate" approaches (brown and purple curves), in which all couplings and energies are computed with the SC as the entire tetramer, are closer to the QM spectra, but the improvement with respect to the light blue spectra is not large, indicating that the perturbation of the H_{inter} term by surrounding monomers is not as important as the perturbation of the H_{intra} term.

As suggested by the similarity between the purple and brown curves, three- and four-monomer CT couplings provide a negligible contribution, except for the negative peak at ∼240 nm. In fact, for one of the tetramers (G1−G2−G3−G4), neglecting the three-/four-monomer terms (brown curves) improves the agreement with the TD-DFT spectra in that region. However, this is most likely due to a cancellation of errors, considering that additional LE and CT states would be necessary to reproduce the high-energy region.

4.2. ECD and Absorption Spectra of Tel21 and TG4T.

As discussed in the previous section, the test calculations on dimers show that six types of CT states are sufficient to include. The tests on trimers and tetramers indicate some approximations in the calculation of some H_{inter} terms, i.e., neglecting three- and four-monomer CT coupling terms, as well as the coupling with distant monomers, have a limited effect on the agreement between FrDEx and reference QM spectra. The computational burden of FrDEx can thus be safely reduced by considering only H_{inter} terms involving adjacent pairs of monomers. On the other hand, the perturbation of H_{intra} due to surrounding monomers has an important impact, and its inclusion can increase the accuracy of the FrDEx spectra. We shall exploit these indications when computing the spectra of Tel21 and TG4T.

The experimental ECD spectra of these two GQs (see Figure 7) are very different, illustrating why this technique is a major source of information on the GQ topology. For Tel21, we have a positive lobe peaking at 290−300 nm and a negative one, slightly more intense, peaking above 260 nm. A third positive peak is found at ∼240 nm. For TG4T, a strong positive peak at 260 nm is followed by a less intense negative one at 240 nm. The TD-DFT spectra are in good agreement with the experimental ones with respect to the energy difference and the relative intensity of the different peaks. The absolute intensity of the TD-DFT and experimental spectra are however different. This could be partially attributed to nucleobase/counter-ion concentration in the experimental spectra and how the resulting ECD signal is normalized with respect to the nucleobase concentration. A discussion of these points is beyond the scope of this paper, and we refer the reader to ref 54. Besides the points just mentioned, the discrepancy with the experimental absolute intensities can be due to the limitations of the QM calculations (functional, basis set, solvent model), in addition to the approximations in the computational/molecular model (namely, lack of inclusion of the other nucleobases and counterions) and the fact that only one structure is used for each TD-DFT spectrum, without including thermal fluctuations and vibrational effects.[55]

FHC calculations can reproduce the qualitative differences in the ECD spectra of the 2-folds.[39,40,58] However, several important differences with respect to the experimental (and reference QM) ones appear. The FHC spectra are blue-shifted, and, more importantly, the relative intensity of the different peaks is not correctly predicted. In particular, the

https://dx.doi.org/10.1021/acs.jctc.0c01100
J. Chem. Theory Comput. XXXX, XXX, XXX−XXX

low-energy peak (at ∼280 nm) in Tel21 is ca. 3 times less intense than the negative lobe (at ∼260 nm), whereas they should have a comparable intensity. In contrast, for TG4T the intensity of the two lobes (at ∼260 and ∼240 nm) is too similar.

In the next step of our study, we shall compute the ECD spectra with the FrDEx method. As mentioned in the introduction to this section, the effect of "distant" dimers on the ECD spectra seems limited, and their computation can be neglected without detriment to the results. To define what we mean by distant, we have computed all of the couplings for all of the possible dimers in Tel21 and TG4T. As reported in SI Section S5, either when the stacking distance is >6 Å or when the absolute distance between centroids of the mG bases is >10 Å, all of the coupling terms of H_{inter} (i.e., intermonomer LE−LE couplings and all CT couplings) are very small, which is the reason why their inclusion does not affect the spectra. This distance dependence of the couplings implies that the dimers we consider as distant are those that are separated by more than a tetrad (e.g., G1/G3 for Tel21 as labeled in Figure 1), as well as those that are diagonal to one another (e.g., G1/G11 for Tel21, as labeled in Figure 1). As a definitive check, we report test calculations in the SI (Figure S4), illustrating that these dimers do not affect the spectra. In this way, only 36 dimer diabatizations (instead of 66) for Tel21 and 52 (instead of 120) for TG4T are required.

The spectra obtained with this procedure are reported in Figure 7, with all spectra using dimers as the SC for computing the H_{inter} parameters but different sizes of SC for H_{intra}. These different sizes of SC are illustrated in Figure 6 for Tel21 and explained further in the following. The most economical approach is to use the same dimers for the SC to compute both H_{intra} parameters and H_{inter} parameters. Since a single value is required for the H_{intra} parameters for each monomer, we use an average over the dimers that a particular monomer is involved in. For example, the values of the LE energies and the intrasite couplings of G2 in Tel21 are given as an average over those obtained by diabatizing G2−G1, G2−G3, G2−G4, G2−G5, G2−G6, G2−G7, G2−G8, and G2−G9 dimers.

As reported in Table 1, the averaging procedure provides H_{intra} parameters similar to that of the isolated monomer, so a limited perturbation effect is included in this approach. Nevertheless, a comparison of these spectra for Tel21 and TG4T in Figure 7 (green curves) to the FHC curves shows

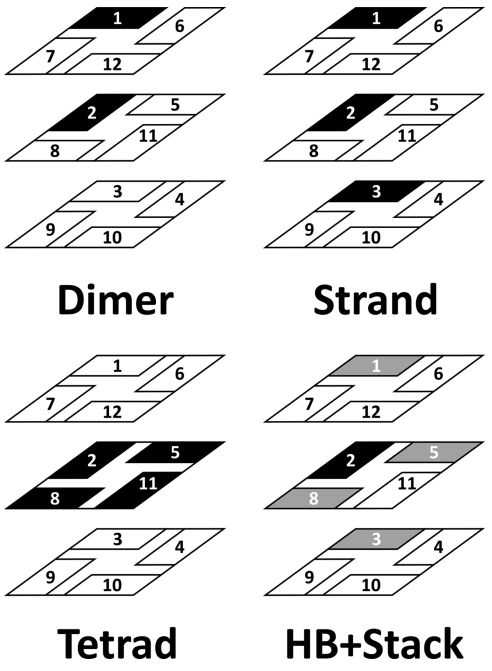

Figure 6. Illustration of different supramolecular complexes chosen for diabatization of Tel21 (colored rectangles). Guanines for which FrDEx parameters are obtained from the specified SC are highlighted in black.

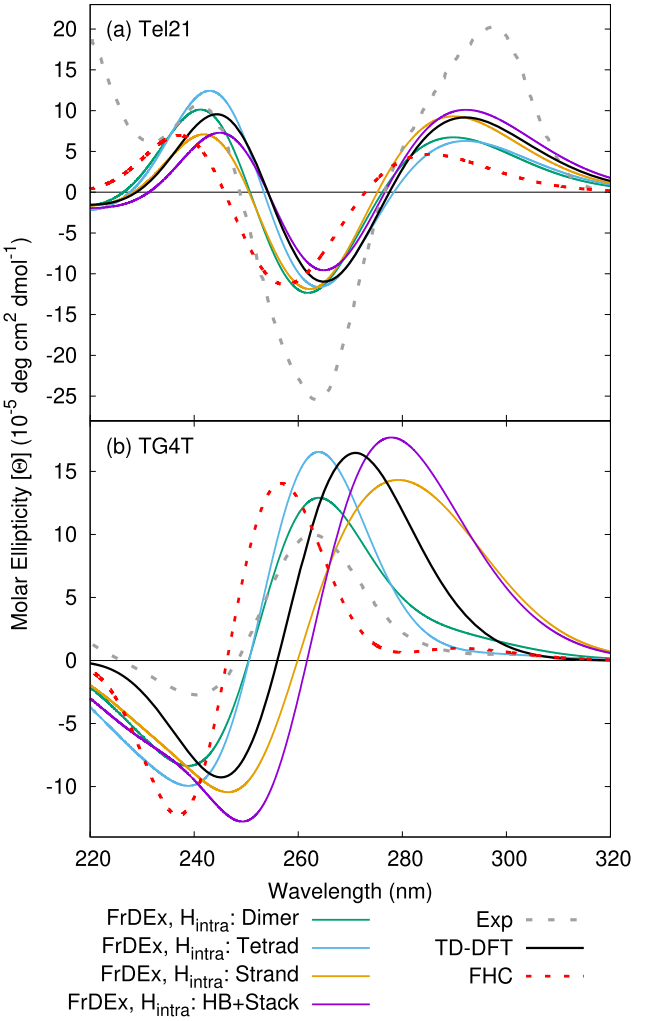

Figure 7. Computed (TD-DFT, FHC, and FrDEx) and experimental[56,57] ECD spectra of (a) Tel21 and (b) TG4T. FrDEx spectra use different sizes of SC to calculate the H_{intra} term of eq 4, while they all use dimers as the SC to calculate H_{inter}. All calculated spectra are shifted by −0.85 eV.

that inclusion of the CT states and the limited perturbation effect red-shifts the main peaks, which get closer to the full QM reference. The accuracy of the computed intensity of the ∼240 nm (the blue-wing lobes) also significantly improves.

The percentage contribution of the CT states to the lowest 24(32) excitonic states for Tel21(TG4T) (i.e., those with predominant LE contribution, most important to the spectra) is shown in SI Section S6.3. The contribution of CT states is significant, also for "key" states, for example, the excitonic

https://dx.doi.org/10.1021/acs.jctc.0c01100
J. Chem. Theory Comput. XXXX, XXX, XXX−XXX

state 1 for Tel21, which is primarily responsible for the red wing of the spectrum.

However, these FrDEx H_{intra}:dimer spectra are still blue-shifted with respect to the TD-DFT ones and the intensity of the red-wing peaks is not completely reproduced. As already discussed, the effect of stacking and hydrogen bonding on the perturbation of H_{intra} is important. Therefore, we consider an SC that includes both of these effects for the computation of H_{intra}, which we refer to as "HB + stack". An example is shown in Figure 6 for G2 in Tel21, with the other Gs included in the SC depicted in gray. The parameters obtained are reported in Table 1, with a significant redshift of the L_a and L_b energies (in particular L_b) and a large L_a−L_b intramonomer coupling. The spectra (purple curves in Figure 7) demonstrate a further redshift compared to the "dimers only" spectra, and an increase in intensity of the red-wing lobe. For Tel21, the QM reference is almost matched, while for TG4T, the redshift and intensity are slightly overestimated. The HB + stack procedure is however rather computationally expensive, since it requires 12/16 additional TD-DFT computations on tetramers or pentamers of mG for Tel21/TG4T (see Table S1 in the SI).

More economical approaches, while still accounting for some of the perturbation of H_{intra}, are to include the effect of either hydrogen bonding or stacking. In the first case, we can use as the SC a hydrogen-bonded tetrad, in a procedure we label as "tetrad". An example of this for the middle tetrad of Tel21 is shown in Figure 6. The advantage of this procedure is that the H_{intra} parameters of four monomers may be obtained simultaneously so that only 3(4) TD-DFT computations on tetrads are necessary for Tel21(TG4T), which has a limited impact on the computational cost (see Table S1 in the SI). The spectra from this approach (light blue curves in Figure 7) do not compare as well to the QM reference as the HB+Stack approach; however, they are in better agreement than the dimers only approach, for a limited extra cost.

In the second case, we can include the effect of the stacking on H_{intra} using the entire stacked strand as SC, labeled as the "strand" approach and illustrated for a strand of Tel21 in Figure 6. Similar to the tetrad approach, the parameters for 3(4) monomers may be obtained simultaneously for Tel21-(TG4T) such that this procedure requires only four additional calculations with respect to the "dimer only" one. The strand approach is expected to be particularly effective when dealing with very closely stacked systems, which could strongly affect H_{intra}. Indeed, the orange spectra in Figure 7 compare reasonably well with the much more expensive HB + stack approach, in particular for the low-energy peak of Tel21. For TG4T, the peak positions are also closely matched, with a small decrease in intensity.

4.2.1. Absorption Spectra. The calculation of the absorption spectra, which are less sensitive to GQ topology, confirms the importance of a proper inclusion of CT couplings and H_{intra} perturbation in the excitonic calculations.

In Figure 8, the absorption spectra computed by the different FrDEx approaches are compared with the FHC, TD-DFT, and experimental[36] ones for Tel21 and TG4T. The spectra of an equimolar solution of mG are also shown in magenta ("TD-DFT sum mon" curves). TD-DFT calculations predict that the formation of the GQ is associated with a weak redshift of the absorption maximum, a significant hypochromic effect (decrease of the absorption intensity) and an increase of the absorption in the red wing, i.e., above 290 nm. The absence of the backbone and of the inner ions (which would lead to an additional redshift of the red wing)[36] makes a comparison with the available experimental results less straightforward, as clearly shown for Tel21, and slightly less obviously seen for TG4T due to the difference in absorption maxima wavelength. On the other hand, it is clear that the FHC spectra do not mimic satisfactorily the QM reference, with a significantly blue-shifted maximum and, especially, a severe underestimation of the absorption in the red wing. For what concerns the hypochromic effect, standard excitonic models are also ill-suited to correctly reproduce this effect. Indeed, as shown in Figure 8, the intensity of the maximum is slightly larger than in the "sum of the monomer" spectra (and the total absorptivity is almost the same). The FrDEx spectra (especially those from the HB + stack SC) are instead in good agreement with the QM reference and reproduce the shifts associated with the GQ formation. In particular, the presence of the red-wing tail is correctly predicted. An interesting point to note is that while the hydrogen-bonding perturbation on H_{intra} with tetrad overestimates the intensity, the stacking perturbation with strand underestimates the intensity, whereas

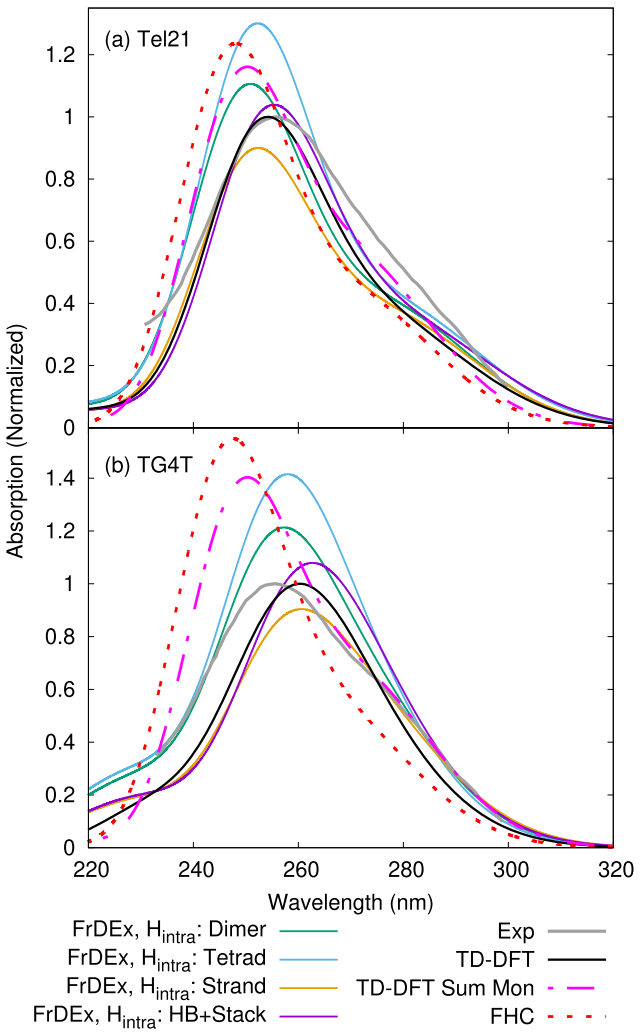

Figure 8. Computed (TD-DFT, FHC, and FrDEx) and experimental[36] absorption spectra of (a) Tel21 and (b) TG4T. The peaks of the experimental and TD-DFT spectra are normalized to 1, while the rest of the calculated spectra use the same normalization factor as TD-DFT. FrDEx spectra use different sizes of SC to calculate the H_{intra} term of eq 4, while they all use dimers as the SC to calculate H_{inter}. All calculated spectra are shifted by −0.85 eV.

https://dx.doi.org/10.1021/acs.jctc.0c01100
J. Chem. Theory Comput. XXXX, XXX, XXX−XXX

HB + stack yields approximately the correct intensity. This result highlights once more that including both stacking and HB effects is crucial to reproduce the intensity of the different transitions.

5. CONCLUDING REMARKS

We here propose a fragment diabatization-based excitonic (FrDEx) model, suitable for strongly coupled MCAs. It is made up of a stand-alone diabatization code and a number of interfaces freely available upon request. The approach relies upon two important features: first, the fragment diabatization itself, which can include more than one LE for each monomer, an arbitrary number of CT states, and an arbitrary number of monomers in the fragment such that many-monomer effects can be included. Second, the excitonic Hamiltonian is split into an H_{intra} term, containing the LE energies and coupling between different LEs on the same monomer, and an H_{inter} term containing all CT energies and couplings, as well as the intermonomer LE−LE couplings. This approach allows different sizes of fragment to be used in the diabatization(s) to parameterize H_{intra} and H_{inter}. In this way, it is easier to find the "best" balance between accuracy and computational cost, as many-monomer effects and different couplings can be switched on and off as required for the problem at hand.

As a first application, we choose a very challenging case for excitonic models, i.e., the computation of the ECD and absorption spectra of two prototype GQs with different folding topologies. FrDEx provides spectra much closer to the QM reference than standard excitonic models that do not include CT states and/or many-monomer perturbative effects. In particular, we have shown that inclusion of CT states is mandatory to correctly reproduce the high-energy region of the spectra and, at the same time, the red-wing tail. Furthermore, our study also highlights another important feature, sometimes overlooked, of chromophores possessing two or more LEs that are close in energy and therefore can easily mix. For these species, the properties and spectral features can be changed by the presence of adjacent chromophores, which act through effects that go beyond an excitonic picture, for example, through hydrogen-bonding interactions. These changes are mirrored in the computed spectra, which are notably different with respect to those obtained by using LE states computed for isolated monomers, as often done in standard excitonic models. Such effects can be taken into account in FrDEx via the H_{intra} term, whose parameters can be altered by surrounding chromophores through suitable choices of the SC adopted in the diabatization. We have explored three different procedures. The most expensive, HB + stack, including both the effect of interbase hydrogen bonding and stacking, is the most accurate one. On the other hand, tetrad, which considers only the effect of hydrogen bonds, and strand, including only the effects of stacking, significantly improves the agreement with QM spectra with a limited additional computational cost. It is clear that other choices of the SC to be used for H_{intra} (and H_{inter}) terms are also possible, depending on the features of the MCA examined.

Prefacing the calculations on the entire GQs, we performed tests on representative smaller subsystems to elucidate the best approach to take with FrDEx. In addition to providing a first indication of the importance of perturbation of the H_{intra} term mentioned above, calculations on dimers permitted the "optimal" number of CT states to be determined. Furthermore, they also highlight that the coupling between distant dimers can be discarded. Calculations on trimers and tetramers illustrated that three- and four-monomer CT coupling terms were not necessary to include and that the perturbative effect on the H_{inter} term was not as important as the H_{intra} term for this system.

These smaller systems also better highlight discrepancies in the FHC approach, which are masked by partial error cancellation due to the multitude of interactions in the full GQ. These failures could, for example, make application of FHC to investigate thermal fluctuations by coupling to molecular dynamics simulations problematic. During the molecular dynamics, a large part of the conformational space could be explored, including "nonstandard" arrangement of the bases, for example, when the stacking distance is rather small or the hydrogen-bonded tetrads are disrupted. These conformations could, in principle, have a remarkable influence on the spectral signal, not properly captured by FHC calculations.

As far as the computational cost is concerned, FrDEx can get accurate spectra being only ∼2 times slower than a simple FHC model, requiring, at the same time, much less computational resources (e.g., memory occupancy) than a full TD-DFT calculation of GQ and being 2−3 times quicker. Moreover, because the diabatization relies on separate calculations, FrDEx is embarrassingly parallel, and this further increases its range of applicability. Finally, (as discussed in SI Figure S5), additional savings could be obtained by exploiting the "quasi-symmetrical" arrangement of some topologies, such as TG4T.

In future work, we aim to use FrDEx in combination with molecular dynamics calculations to study the effect of thermal fluctuations on the spectral properties of GQ (or any other MCA), where snapshots from the molecular dynamics calculations are used with FrDEx computing the spectra at these geometries. This will not only allow conformational averaging but also help us to determine time-dependent processes that affect the spectral signal, such as folding and unfolding. Other possible developments involve the use of QM/MM calculations to treat environmental effects, as well as the inclusion of vibronic contributions.[59,60]

The conclusions of the present study are expected to be of general interest for other strongly coupled MCAs as well as GQ. Thanks to its flexibility, FrDEx thus promises to be a useful tool to disentangle the different effects responsible for the spectral behavior of MCAs and to study their photoactivated processes.

■ ASSOCIATED CONTENT

Supporting Information

The Supporting Information is available free of charge at https://pubs.acs.org/doi/10.1021/acs.jctc.0c01100.

Derivation of the diabatization procedure; equations for the ECD and absorption spectra calculations; additional ECD and absorption spectra; figures displaying the coupling parameters calculated by the FrDEx approach; tabulated data of energies, transition dipole moments, and rotational strengths of excitonic/adiabatic electronic states; tabulated calculation times; and percentage contributions of LE and CT states to FrDEx computations for Tel21 and TG4T (PDF)

https://dx.doi.org/10.1021/acs.jctc.0c01100
J. Chem. Theory Comput. XXXX, XXX, XXX−XXX

AUTHOR INFORMATION

Corresponding Authors

Fabrizio Santoro − *Consiglio Nazionale delle Ricerche, Istituto di Chimica dei Composti Organo Metallici (ICCOM-CNR), SS di Pisa, Area della Ricerca, I-56124 Pisa, Italy;* orcid.org/0000-0003-4402-2685; Email: fabrizio.santoro@pi.iccom.cnr.it

Roberto Improta − *Consiglio Nazionale delle Ricerche, Istituto di Biostrutture e Bioimmagini (IBB-CNR), I-80136 Napoli, Italy;* orcid.org/0000-0003-1004-195X; Email: robimp@unina.it

Authors

James A. Green − *Consiglio Nazionale delle Ricerche, Istituto di Biostrutture e Bioimmagini (IBB-CNR), I-80136 Napoli, Italy;* orcid.org/0000-0002-5036-3104

Haritha Asha − *Consiglio Nazionale delle Ricerche, Istituto di Biostrutture e Bioimmagini (IBB-CNR), I-80136 Napoli, Italy*

Complete contact information is available at: https://pubs.acs.org/10.1021/acs.jctc.0c01100

Notes

The authors declare no competing financial interest.

ACKNOWLEDGMENTS

This project has received funding from the European Union's Horizon 2020 Research and Innovation Programme under the Marie Sklodowska-Curie grant agreement no. 765266 (LightDyNAmics). The authors thank Dr. Lara Martínez-Fernández for useful discussions.

REFERENCES

(1) van Amerongen, H.; van Grondelle, R.; Valkunas, L. *Photosynthetic Excitons*; World Scientific, 2000.

(2) Curutchet, C.; Mennucci, B. Quantum Chemical Studies of Light Harvesting. *Chem. Rev.* **2017**, *117*, 294−343.

(3) Mirkovic, T.; Ostroumov, E. E.; Anna, J. M.; van Grondelle, R.; Govindjee; Scholes, G. D. Light Absorption and Energy Transfer in the Antenna Complexes of Photosynthetic Organisms. *Chem. Rev.* **2017**, *117*, 249−293.

(4) Cheng, Y.-C.; Fleming, G. R. Dynamics of Light Harvesting in Photosynthesis. *Annu. Rev. Phys. Chem.* **2009**, *60*, 241−262.

(5) Segatta, F.; Cupellini, L.; Garavelli, M.; Mennucci, B. Quantum Chemical Modeling of the Photoinduced Activity of Multichromophoric Biosystems. *Chem. Rev.* **2019**, *119*, 9361−9380.

(6) Spano, F. C. Excitons In Conjugated Oligomer Aggregates, Films, And Crystals. *Annu. Rev. Phys. Chem.* **2006**, *57*, 217−243.

(7) Hestand, N. J.; Spano, F. C. Expanded Theory of H- and J-Molecular Aggregates: The Effects of Vibronic Coupling and Intermolecular Charge Transfer. *Chem. Rev.* **2018**, *118*, 7069−7163.

(8) Krueger, B. P.; Scholes, G. D.; Fleming, G. R. Calculation of Couplings and Energy-Transfer Pathways between the Pigments of LH2 by the ab Initio Transition Density Cube Method. *J. Phys. Chem. B* **1998**, *102*, 5378−5386.

(9) Scholes, G. D.; Gould, I. R.; Cogdell, R. J.; Fleming, G. R. Ab Initio Molecular Orbital Calculations of Electronic Couplings in the LH2 Bacterial Light-Harvesting Complex of Rps-Acidophila. *J. Phys. Chem. B* **1999**, *103*, 2543−2553.

(10) Iozzi, M. F.; Mennucci, B.; Tomasi, J.; Cammi, R. Excitation energy transfer (EET) between molecules in condensed matter: A novel application of the polarizable continuum model (PCM). *J. Chem. Phys.* **2004**, *120*, 7029−7040.

(11) Förster, T. Zwischenmolekulare Energiewanderung und Fluoreszenz. *Ann. Phys.* **1948**, *437*, 55−75.

(12) Tamura, H.; Burghardt, I.; Tsukada, M. Exciton Dissociation at Thiophene/Fullerene Interfaces: The Electronic Structures and Quantum Dynamics. *J. Phys. Chem. C* **2011**, *115*, 10205−10210.

(13) Tamura, H.; Burghardt, I. Potential Barrier and Excess Energy for Electron−Hole Separation from the Charge-Transfer Exciton at Donor−Acceptor Heterojunctions of Organic Solar Cells. *J. Phys. Chem. C* **2013**, *117*, 15020−15025.

(14) Tamura, H. Diabatization for Time-Dependent Density Functional Theory: Exciton Transfers and Related Conical Intersections. *J. Phys. Chem. A* **2016**, *120*, 9341−9347.

(15) Polkehn, M.; Tamura, H.; Burghardt, I. Impact of charge-transfer excitons in regioregular polythiophene on the charge separation at polythiophene-fullerene heterojunctions. *J. Phys. B: At., Mol. Opt. Phys.* **2017**, *51*, No. 014003.

(16) Polkehn, M.; Eisenbrandt, P.; Tamura, H.; Burghardt, I. Quantum dynamical studies of ultrafast charge separation in nanostructured organic polymer materials: Effects of vibronic interactions and molecular packing. *Int. J. Quantum Chem.* **2018**, *118*, No. e25502.

(17) Popp, W.; Polkehn, M.; Hughes, K. H.; Martinazzo, R.; Burghardt, I. Vibronic coupling models for donor-acceptor aggregates using an effective-mode scheme: Application to mixed Frenkel and charge-transfer excitons in oligothiophene aggregates. *J. Chem. Phys.* **2019**, *150*, No. 244114.

(18) Popp, W.; Polkehn, M.; Binder, R.; Burghardt, I. Coherent Charge Transfer Exciton Formation in Regioregular P3HT: A Quantum Dynamical Study. *J. Phys. Chem. Lett.* **2019**, *10*, 3326−3332.

(19) Li, X.; Parrish, R. M.; Liu, F.; Kokkila Schumacher, S. I. L.; Martínez, T. J. An Ab Initio Exciton Model Including Charge-Transfer Excited States. *J. Chem. Theory Comput.* **2017**, *13*, 3493−3504.

(20) Nottoli, M.; Jurinovich, S.; Cupellini, L.; Gardiner, A. T.; Cogdell, R.; Mennucci, B. The role of charge-transfer states in the spectral tuning of antenna complexes of purple bacteria. *Photosynth. Res.* **2018**, *137*, 215−226.

(21) Cupellini, L.; Caprasecca, S.; Guido, C. A.; Müh, F.; Renger, T.; Mennucci, B. Coupling to Charge Transfer States is the Key to Modulate the Optical Bands for Efficient Light Harvesting in Purple Bacteria. *J. Phys. Chem. Lett.* **2018**, *9*, 6892−6899.

(22) Cupellini, L.; Calvani, D.; Jacquemin, D.; Mennucci, B. Charge transfer from the carotenoid can quench chlorophyll excitation in antenna complexes of plants. *Nat. Commun.* **2020**, *11*, No. 662.

(23) Phan, A. T.; Mergny, J. Human telomeric DNA: G-quadruplex, i-motif and Watson−Crick double helix. *Nucleic Acids Res.* **2002**, *30*, 4618−4625.

(24) Phan, A. T. Human telomeric G-quadruplex: structures of DNA and RNA sequences. *FEBS J.* **2010**, *277*, 1107−1117.

(25) Rhodes, D.; Lipps, H. J. G-quadruplexes and their regulatory roles in biology. *Nucleic Acids Res.* **2015**, *43*, 8627−8637.

(26) Yang, D.; Lin, C. *G-Quadruplex Nucleic Acids: Methods and Protocols*; Humana: New York, NY, 2019.

(27) Vorlíčková, M.; Kejnovská, I.; Sagi, J.; Renčiuk, D.; Bednářová, K.; Motlová, J.; Kypr, J. Circular dichroism and guanine quadruplexes. *Methods* **2012**, *57*, 64−75.

(28) Vorlíčková, M.; Kejnovská, I.; Bednářová, K.; Renčiuk, D.; Kypr, J. Circular Dichroism Spectroscopy of DNA: From Duplexes to Quadruplexes. *Chirality* **2012**, *24*, 691−698.

(29) del Villar-Guerra, R.; Trent, J. O.; Chaires, J. B. G-Quadruplex Secondary Structure Obtained from Circular Dichroism Spectroscopy. *Angew. Chem., Int. Ed.* **2018**, *57*, 7171−7175.

(30) Randazzo, A.; Spada, G. P.; da Silva, M. W. *Quadruplex Nucleic Acids*; Chaires, J. B.; Graves, D., Eds.; Springer: Berlin, Heidelberg, 2013; pp 67−86.

(31) Harada, N.; Nakanishi, K. Optical rotatory power of the benzoate group. *J. Am. Chem. Soc.* **1968**, *90*, 7351−7352.

(32) Harada, N.; Chen, S.-M. L.; Nakanishi, K. Quantitative definition of exciton chirality and the distant effect in the exciton chirality method. *J. Am. Chem. Soc.* **1975**, *97*, 5345−5352.

(33) Harada, N.; Nakanishi, K.; Berova, N. *Comprehensive Chiroptical Spectroscopy*; Berova, N.; Polavarapu, P. L.; Nakanishi, K.; Woody, R. W., Eds.; Wiley, 2012; pp 115−166.
(34) Pescitelli, G.; Di Bari, L.; Berova, N. Application of electronic circular dichroism in the study of supramolecular systems. *Chem. Soc. Rev.* **2014**, *43*, 5211−5233.
(35) Improta, R. Quantum Mechanical Calculations Unveil the Structure and Properties of the Absorbing and Emitting Excited Electronic States of Guanine Quadruplex. *Chem. - Eur. J.* **2014**, *20*, 8106−8115.
(36) Martínez-Fernández, L.; Esposito, L.; Improta, R. Studying the excited electronic states of guanine rich DNA quadruplexes by quantum mechanical methods: main achievements and perspectives. *Photochem. Photobiol. Sci.* **2020**, *19*, 436−44.
(37) Albano, G.; Pescitelli, G.; Di Bari, L. Chiroptical Properties in Thin Films of π-Conjugated Systems. *Chem. Rev.* **2020**, *120*, 10145−10243.
(38) Swathi, K.; Sissa, C.; Painelli, A.; George Thomas, K. Supramolecular chirality: a caveat in assigning the handedness of chiral aggregates. *Chem. Commun.* **2020**, *56*, 8281−8284.
(39) Loco, D.; Jurinovich, S.; Bari, L. D.; Mennucci, B. A fast but accurate excitonic simulation of the electronic circular dichroism of nucleic acids: how can it be achieved? *Phys. Chem. Chem. Phys.* **2016**, *18*, 866−877.
(40) Jurinovich, S.; Cupellini, L.; Guido, C. A.; Mennucci, B. EXAT: EXcitonic analysis tool. *J. Comput. Chem.* **2018**, *39*, 279−286.
(41) Jurinovich, S.; Pescitelli, G.; Di Bari, L.; Mennucci, B. A TDDFT/MMPol/PCM model for the simulation of exciton-coupled circular dichroism spectra. *Phys. Chem. Chem. Phys.* **2014**, *16*, 16407−16418.
(42) Jurinovich, S.; Guido, C. A.; Bruhn, T.; Pescitelli, G.; Mennucci, B. The role of magnetic−electric coupling in exciton-coupled ECD spectra: the case of bis-phenanthrenes. *Chem. Commun.* **2015**, *51*, 10498−10501.
(43) Yaghoubi Jouybari, M.; Liu, Y.; Improta, R.; Santoro, F. Ultrafast Dynamics of the Two Lowest Bright Excited States of Cytosine and 1-Methylcytosine: A Quantum Dynamical Study. *J. Chem. Theory Comput.* **2020**, *16*, 5792−5808.
(44) Voityuk, A. A. Electronic Couplings for Photoinduced Electron Transfer and Excitation Energy Transfer Computed Using Excited States of Noninteracting Molecules. *J. Phys. Chem. A* **2017**, *121*, 5414−5419.
(45) Tomasi, J.; Mennucci, B.; Cammi, R. Quantum Mechanical Continuum Solvation Models. *Chem. Rev.* **2005**, *105*, 2999−3094.
(46) Frisch, M. J.; Trucks, G. W.; Schlegel, H. B.; Scuseria, G. E.; Robb, M. A.; Cheeseman, J. R.; Scalmani, G.; Barone, V.; Petersson, G. A.; et al. *Gaussian 16*, revision C.01; Gaussian Inc.: Wallingford, CT, 2016.
(47) Wang, Y.; Patel, D. J. Solution structure of the human telomeric repeat d[AG3(T2AG3)3] G-tetraplex. *Structure* **1993**, *1*, 263−282.
(48) Laughlan, G.; Murchie, A.; Norman, D.; Moore, M.; Moody, P.; Lilley, D.; Luisi, B. The high-resolution crystal structure of a parallel-stranded guanine tetraplex. *Science* **1994**, *265*, 520−524.
(49) Martínez-Fernández, L.; Banyasz, A.; Markovitsi, D.; Improta, R. Topology Controls the Electronic Absorption and Delocalization of Electron Holes in Guanine Quadruplexes. *Chem. - Eur. J.* **2018**, *24*, 15185−15189.
(50) Law, Y. K.; Hassanali, A. A. Role of Quantum Vibrations on the Structural, Electronic, and Optical Properties of 9-Methylguanine. *J. Phys. Chem. A* **2015**, *119*, 10816−10827.
(51) Improta, R.; Santoro, F.; Blancafort, L. Quantum mechanical studies on the Photophysics and the Photochemistry of nucleic acids and nucleobases. *Chem. Rev.* **2016**, *116*, 3540−3593.
(52) Nogueira, J. J.; Plasser, F.; Gonzaález, L. Electronic delocalization, charge transfer and hypochromism in the UV absorption spectrum of polyadenine unravelled by multiscale computations and quantitative wavefunction analysis. *Chem. Sci.* **2017**, *8*, 5682−5691.
(53) Plasser, F. TheoDORE: A toolbox for a detailed and automated analysis of electronic excited state computations. *J. Chem. Phys.* **2020**, *152*, No. 084108.
(54) del Villar-Guerra, R.; Gray, R. D.; Chaires, J. B. Characterization of Quadruplex DNA Structure by Circular Dichroism. *Curr. Protoc. Nucleic Acid Chem.* **2017**, *68*, 17.8.1−17.8.16.
(55) Cupellini, L.; Lipparini, F.; Cao, J. Absorption and Circular Dichroism Spectra of Molecular Aggregates With the Full Cumulant Expansion. *J. Phys. Chem. B* **2020**, *124*, 8610−8617.
(56) Xu, Y.; Noguchi, Y.; Sugiyama, H. The new models of the human telomere d[AGGG(TTAGGG)3] in K+ solution. *Bioorg. Med. Chem.* **2006**, *14*, 5584−5591.
(57) Petraccone, L.; Erra, E.; Esposito, V.; Randazzo, A.; Mayol, L.; Nasti, L.; Barone, G.; Giancola, C. Stability and Structure of Telomeric DNA Sequences Forming Quadruplexes Containing Four G-Tetrads with Different Topological Arrangements. *Biochemistry* **2004**, *43*, 4877−4884.
(58) Gattuso, H.; Spinello, A.; Terenzi, A.; Assfeld, X.; Barone, G.; Monari, A. Circular Dichroism of DNA G-Quadruplexes: Combining Modeling and Spectroscopy To Unravel Complex Structures. *J. Phys. Chem. B* **2016**, *120*, 3113−3121.
(59) Padula, D.; Santoro, F.; Pescitelli, G. A simple dimeric model accounts for the vibronic ECD spectra of chiral polythiophenes in their aggregated states. *RSC Adv.* **2016**, *6*, 37938−37943.
(60) Menger, M. F. S. J.; Plasser, F.; Mennucci, B.; González, L. Surface Hopping within an Exciton Picture. An Electrostatic Embedding Scheme. *J. Chem. Theory Comput.* **2018**, *14*, 6139−6148.

https://dx.doi.org/10.1021/acs.jctc.0c01100
J. Chem. Theory Comput. XXXX, XXX, XXX−XXX